

Thermodynamic model of solid non-stoichiometric uranium dioxide

E Yakub^{1,2}, C Ronchi¹ and I Iosilevski³

¹ European Commission, Joint Research Centre, Institute for Transuranium Elements, PO Box 2340, D-76125 Karlsruhe, Germany

² Computer Science Department, Odessa State Economic University, Odessa, Ukraine

³ Moscow Institute of Physics and Technology, State University, Moscow, Russia

Received 10 June 2005, in final form 25 November 2005

Published 11 January 2006

Online at stacks.iop.org/JPhysCM/18/1227

Abstract

A new equation of state for solid UO_{2+x} is presented, based on an extended ionic model. A thermodynamic description of the imperfect and non-stoichiometric ionic solid is obtained accounting for short- and long-ranged inter-ionic forces, as well as for formation of Frenkel defects. Both Coulomb and short-range interactions between defects are encompassed in a highly non-ideal ionic system where interactions of Frenkel defects are taken into account explicitly as short-ranged interactions of quasi-dipoles. A simplified analytical form for the free energy of the perfect anharmonic crystal was obtained and then combined with additional contributions from formation and interaction of defects. By fitting a few numerical constants, the variations of thermodynamic properties of UO_{2+x} are predicted as functions of temperature, density and stoichiometry. The model describes the pre-melting transition into the superionic state in solid stoichiometric UO_2 and predicts the behaviour of the transition line in the non-stoichiometric domain.

1. Introduction

In the current Sixth Framework Programme of the European Commission, under the thematic priority ‘Safety of nuclear fuel’, the high temperature thermodynamic properties of uranium dioxide are being investigated in the Joint Research Centre. Though this matter is of primary importance for current reactor accident analysis, insufficient data are available not only for complex thermochemical systems including fuel and structural materials, but also for the simpler non-stoichiometric uranium dioxide system. For instance, recent results of melting experiments on hyperstoichiometric uranium dioxide, carried out with new, advanced techniques [1, 2], provide evidence for relevant differences of the solidus and liquidus curves compared with the scanty pre-existing data obtained more than three decades ago [3]. If one considers that the current thermodynamic models for the high temperature behaviour of the

solid solution UO_{2+x} [4, 5] have been constructed by fitting these old, probably inaccurate data, it appears that a realistic equation of state (EOS) of this system based on wide ranging assumptions is necessary to consolidate the resultant new views. The work reported in this paper represents a first step towards a more accurate definition of the high temperature phase diagram and thermodynamic properties of non-stoichiometric uranium dioxide.

For the description and extrapolation of experimental data in solid phases of pure metals, ionic and molecular crystals at high temperatures, equations of state are mostly utilized, based on the well known Mie–Grüneisen approach [6]. However, these phenomenological EOSs cannot be directly applied to multi-component systems such as non-stoichiometric compounds or metallic alloys, since this approach is essentially limited by the constraint of constant composition. On the other hand, the thermodynamic properties of non-stoichiometric oxides, especially their phase diagram, demonstrate unusually complex behaviour (see the excellent review in [7]) and require more sophisticated methods for description and explanation. Furthermore, ionic crystals at high temperatures may be effectively imperfect even under stoichiometric conditions, for instance, by exhibiting peculiar features such as a phase transition into a superionic state at a temperature somewhat below the melting point. This transition is caused by the increasing instability in the oxygen sub-lattice with temperature, and is closely related to changes in the formation energy of Frenkel defects. Simple models for description of this transition have been formulated in terms of the ideal lattice gas [7] or Debye–Hückel approximation [8, 9] and, therefore, are intrinsically deficient in describing real ionic solids near their melting point. Owing to the complexity of the problem, a wide-range EOS for these solids is still missing.

The aim of this paper is to demonstrate the applicability of an alternative approach, essentially based on statistical thermodynamics of solids, which can be extended to non-stoichiometric compounds and used for explanation and prediction of their phase behaviour.

Based on the previous considerations, it appears that the thermodynamic properties of $\text{UO}_{2\pm x}$ are mostly defined by the features of the anion sub-lattice and by the cation capability to adapt the valence to the given oxygen defect configurations. In this respect, the more energetic cation vacancies and interstitials are expected to play a secondary role—which is also confirmed by the analysis of the high temperature behaviour of the heat capacity that can be almost entirely interpreted in terms of oxygen defect formation. For large hyperstoichiometry compositions, approaching the high temperature boundary of the fcc solid solution, it might be necessary to consider additional aspects connected with the emergent role of $\text{U}^{(6+)}$. However, experimental data in this domain are missing, so that a self-consistent equation of state accounting for sole oxygen defects provides the most appropriate ground for possible extensions, if these are needed. Therefore, a simplified analytical form of such an EOS is presented, which, after fitting of few numerical constants, does reasonably well reproduce the solid-state properties of non-stoichiometric UO_{2+x} , including the pre-melting transition. Density, enthalpy, entropy, heat capacity, compressibility and thermal expansion of solid $\text{UO}_{2\pm x}$ as well as the oxygen potential are calculated in a wide range of temperature and stoichiometry $x = \text{O/U} - 2$ and compared with existing experimental data and computer simulations of solid $\text{UO}_{2\pm x}$. Furthermore, if combined with recent theoretical models for the uranium dioxide fluid state, it can be used to predict liquid/solid and vapour/solid equilibrium [10].

2. Composite model EOS for non-stoichiometric solid

Solid uranium dioxide is known to behave as an essentially ionic system, which can be treated as a fluorite lattice occupied by uranium cations $\text{U}^{(n+)}$, $n = 3, 4, 5$, and doubly charged

Table 1. Components of the chemical model for imperfect and non-stoichiometric $\text{UO}_{2\pm x}$.

Index		Component description	N_i/N_U
0	V_L	Oxygen lattice vacancy	φ
1	$O_i^{(2-)}$	Interstitial oxygen anion	$\varphi + x$
2	$O_L^{(2-)}$	Oxygen on lattice site	$2 - \varphi$
3	$U^{(3+)}$	Trivalent uranium cation	$\varepsilon - x$
4	$U^{(4+)}$	Tetravalent uranium cation	$1 - 2\varepsilon$
5	$U^{(5+)}$	Pentavalent uranium cation	$\varepsilon + x$
6	V_i	Non-occupied interstitial site	$1 - \varphi - x$

oxygen anions $O^{(2-)}$ [7]. We shall use here the form of the free-energy equation of state, which was successfully applied to fluid urania [11]. Its salient features are summarized as follows:

Oxygen enrichment ($x > 0$) or depletion ($x < 0$) of crystalline UO_2 creates a solid solution UO_{2+x} with at least two new features:

- additional vacancies (at $x < 0$) or additional interstitial ions (at $x > 0$);
- more $U^{(3+)}$ at $x < 0$ or more $U^{(5+)}$ (at $x > 0$).

In table 1 are presented the adopted notations. The last column contains the expressions for the concentrations of all components in terms of three independent variables:

- non-stoichiometry parameter x ,
- concentration of vacancies φ , and
- electronic excitation parameter ε describing the equilibrium in the disproportionation $U^{(5+)}/U^{(3+)}$ (see equation (8) below).

The Helmholtz free energy (per uranium ion) of the imperfect non-stoichiometric UO_{2+x} within the composite chemical model [11] consists of contributions from ideal lattice gas⁴, Coulomb and repulsive forces:

$$F(T, \rho, x, \varphi, \varepsilon) = F_{\text{lat}}^{(\text{id})} + \Delta F^{(\text{C})} + \Delta F^{(\text{R})}, \quad (1)$$

T is temperature; $\rho = N_U/V$ is the number density. Both Coulomb and short-range contributions in equation (1) respectively contain two different terms:

$$\begin{aligned} \Delta F^{(\text{C})} &= \Delta F_0^{(\text{C})} + \Delta F_{x,\varphi,\varepsilon}^{(\text{C})}, & \text{and} \\ \Delta F^{(\text{R})} &= \Delta F_0^{(\text{R})} + \Delta F_{x,\varphi,\varepsilon}^{(\text{R})}. \end{aligned}$$

The first contributions $\Delta F_0^{(\text{C})}$ and $\Delta F_0^{(\text{R})}$ account for the interactions of ions placed in perfect lattice sites and are, conceptually, the same as in a perfect crystal. The terms $\Delta F_{x,\varphi,\varepsilon}^{(\text{C})}$ and $\Delta F_{x,\varphi,\varepsilon}^{(\text{R})}$ express the Coulomb and short-range interactions of defects.

Explicit expressions for these contributions to the free energy of a non-stoichiometric solid are presented and discussed below. Equations for pressure P (compressibility factor Z), entropy S , internal energy E , thermal expansion α_T , isothermal β_T and adiabatic compressibility β_S as well as isochoric C_V and isobaric C_P heat capacities may be derived from the above equations through standard thermodynamic relations.

⁴ Hereinafter, ‘ideal’ means ‘non-interacting’, whilst we shall use the term ‘imperfect’ for a lattice containing defects.

3. Defect formation and disproportionation equilibrium

The free energy of an ideal but imperfect lattice gas for one uranium ion can be written in the form

$$-\beta F_{\text{lat}}^{(\text{id})} = (3+x) \ln \rho + (\varepsilon - x) \ln Q_{\text{U}}^{(3+)} + (1-2\varepsilon) \ln Q_{\text{U}}^{(4+)} + (\varepsilon + x) \ln Q_{\text{U}}^{(5+)} + (2+x) \ln Q_{\text{O}}^{(2-)} + \delta S_{\text{lat}}, \quad (2)$$

where $\beta = (kT)^{-1}$ is the inverse temperature, k is the Boltzmann constant,

$$\delta S_{\text{lat}} = 2 \ln 2 - 3 - \sum_{i=0}^6 y_i \ln y_i \quad (3)$$

is the additional contribution to entropy, y_i ($i = 0, \dots, 6$) are the concentrations of all the components defined in the last column of table 1, and $Q_i^{(\pm Z_i)}$ are the ionic internal partition functions.

Since φ and ε are internal variables of the model, their values may be determined directly from the minimum of the Helmholtz free energy:

$$\begin{aligned} \frac{\partial F(T, \rho, x, \varphi, \varepsilon)}{\partial \varphi} &= 0; \\ \frac{\partial F(T, \rho, x, \varphi, \varepsilon)}{\partial \varepsilon} &= 0. \end{aligned} \quad (4)$$

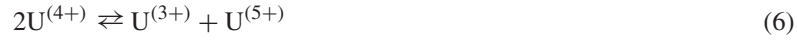
The variational equation (4) leads to mass action law equations for two independent reactions:

- formation of Frenkel defects,



and

- uranium disproportionation,



in the following form:

$$\frac{\varphi(\varphi + x)}{(2 - \varphi)(1 - \varphi - x)} = K_{\varphi}(T, \rho, x, \varphi, \varepsilon), \quad (7)$$

$$\frac{\varepsilon^2 - x^2}{(1 - 2\varepsilon)^2} = K_{\varepsilon}(T, \rho, x, \varphi, \varepsilon). \quad (8)$$

Here

$$K_{\varphi} = \exp \left\{ -\beta \frac{\partial(\Delta F^{(\text{C})} + \Delta F^{(\text{R})})}{\partial \varphi} \right\} \quad (9)$$

and

$$K_{\varepsilon} = \frac{Q_{\text{U}}^{(3+)} Q_{\text{U}}^{(5+)}}{(Q_{\text{U}}^{(4+)})^2} \exp \left\{ -\beta \frac{\partial(\Delta F^{(\text{C})} + \Delta F^{(\text{R})})}{\partial \varepsilon} \right\} \quad (10)$$

are ‘equilibrium constants’ of defect formation and disproportionation reactions, which are actually implicit functions of temperature, density and elemental composition of solid.

According to the conventional quasi-chemical approach (see, e.g., [7, 12]), the equilibrium constants $K_{\text{i}} = \{K_{\varphi}, K_{\varepsilon}\}$ are presumed to depend on temperature only,

i.e. $\ln K_i = H_i/RT + S_i/R$; the quantities H_i and S_i correspond to empirical constants⁵ that are treated as heat and entropy of reaction.

On the other side, according to the variational method, one can calculate the equilibrium constants equations (9) and (10) along with all other properties of an imperfect solid, by knowing the same set of model parameters.

4. Oxygen potential

The central point in the investigation of non-stoichiometric oxides is the determination of the so-called ‘oxygen potential’

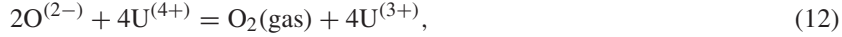
$$\Delta G_{O_2} = RT \ln P_{O_2}, \quad (11)$$

which is simply related to the usual chemical potential of molecular oxygen:

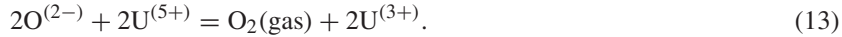
$$\Delta G_{O_2} = \mu_{O_2} - \mu_{O_2}^0.$$

Here $\mu_{O_2}^0$ is the ideal-gas value of the chemical potential at a given temperature and standard pressure ($P = 1$ bar).

The oxygen potential can easily be derived in terms of ionic chemical potentials if one considers the reaction related to the evaporation of oxygen [12]:



or from the above equation of disproportionation equilibrium reaction:



The last equations imply

$$\mu_{O_2} = 2\mu_{O^{(2-)}} + 4\mu_{U^{(4+)}} - 4\mu_{U^{(3+)}} \quad (14)$$

or

$$\mu_{O_2} = 2\mu_{O^{(2-)}} + 2\mu_{U^{(5+)}} - 2\mu_{U^{(3+)}}. \quad (15)$$

All the chemical potentials on the right side of this equation can be derived straightforwardly from the free energy equation. One can also express the oxygen chemical potential using the $T, \rho, x, \varphi, \varepsilon$ variables as follows:

$$\mu_{O_2} = 2 \frac{\partial F(T, \rho, x, \varphi, \varepsilon)}{\partial x}. \quad (16)$$

From substituting the above equations into equation (11) one finally gets the general expression for the pressure of molecular oxygen in terms of the adopted EOS:

$$\begin{aligned} \ln P_{O_2} &= -\beta \mu_{O_2}^0 + 2\beta \frac{\partial F(T, \rho, x, \varphi, \varepsilon)}{\partial x} \\ &= \beta G_0(T) - 2 \ln \rho + \ln \left[\frac{(\varepsilon + x)(\varphi + x)}{(\varepsilon - x)(1 - \varphi - x)} \right] \\ &\quad + 2 \left[\frac{\partial \beta \Delta F^{(C)}}{\partial x} + \frac{\partial \beta \Delta F^{(R)}}{\partial x} \right]. \end{aligned} \quad (17)$$

Here we have

$$\beta G_0(T) = \ln Q_{O_2} - 1 + 2 \ln \left[\frac{Q_U^{(5+)} Q_U^{(2-)}}{Q_U^{(3+)}} \right]. \quad (18)$$

⁵ To be determined from experimental data on vacancy formation or oxygen equilibrium partial pressure.

5. Short-range and Coulomb contributions for ideal solid

The EOS for a perfect one-component crystal with short-range particle interactions is very well known. Due to the importance of anharmonic effects at high temperatures we adopt here the expression for the free energy [13]

$$F = F_{\text{lat}}^{(\text{id})} + U^{(0)} - NkT \ln(v_{\text{f}}/v) - NW + \dots \quad (19)$$

and pressure

$$P = P^{(0)} + kT/v + kT \frac{\partial}{\partial v} \ln(v_{\text{f}}/v) + \frac{\partial}{\partial v} W + \dots, \quad (20)$$

where $F_{\text{lat}}^{(\text{id})}$ is the ‘ideal-lattice’ free energy of non-interacting particles placed into sites of a static lattice, U_0 is the energy of the static lattice and

$$P^{(0)} = -\frac{\partial U^{(0)}}{\partial V} \quad (21)$$

is the so-called ‘cold pressure’, created by forces acting between particles fixed in the static lattice. The term W indicates a pair correlation coefficient that will be discussed below.

The first-order thermal contributions of pressure and free energy are defined in terms of the ‘free volume’ function:

$$v_{\text{f}} = \int \exp\{-\beta U_{1,0}(\vec{x})\} d\vec{x}. \quad (22)$$

Here $\vec{x} = |\vec{q} - \vec{q}^{(0)}|$ is a particle displacement vector, and the integration is carried over all possible displacements of a particle from the lattice site; $U_{1,0}(\vec{x})$ is the one-particle potential energy within an elementary cell. The free volume is a function both of density and temperature, and plays a key role in the theory of thermodynamic properties of crystals [16] as well as in approximate quasi-crystalline theories of liquids [17].

Second-order corrections to the free energy are expressed through pair correlation terms \tilde{W} , which are nearly constant and contribute mainly to entropy [13].

Near the melting point, the anharmonic effects are very important even in a perfect crystal [13], but some principal features of their thermal behaviour can be understood by using the so-called quasi-harmonic approximation [16], where the free volume is a simple power function of the elastic constant $\alpha(\rho)$:

$$v_{\text{f}}^{(h)} = \left(\frac{\pi kT}{\alpha(\rho)} \right)^{3/2}. \quad (23)$$

Anharmonic contributions principally affect thermal expansion and heat capacity, whose properties may be described [13], within a first order theory, by using (even for highly anharmonic crystals) only one or two terms in the expansion of the free volume in powers of temperature:

$$v_{\text{f}} = v_{\text{f}}^{(h)} \left(1 + a_1(\rho) T + a_2(\rho) T^2 + \dots \right). \quad (24)$$

A general formulation of the anharmonic corrections for arbitrary inter-particle potentials, as derived in [13], can be obtained if the inter-particle potential is known. We adopted⁶ the following approximation for the logarithm of the free volume function:

$$\ln v_{\text{f}} = \ln v_{\text{f}}^{(h)} + a_1(\rho) T + \left(a_2(\rho) + 1/2 a_1(\rho)^2 \right) T^2 + \dots \quad (25)$$

⁶ We neglect here the explicit dependence of elastic constant on slow-varying Coulomb forces.

For the inverse-power inter-ionic repulsion potential

$$\Phi^{(R)}(r) = \frac{A_n}{r^n} \quad (26)$$

the reduced free energy $\beta F_0^{(R)}$ is one parametric, depending only on the variable $z = \{\beta\alpha^*(\rho)\}^{-1}$.

Hence the resulting equation for the repulsive contribution to the EOS of the ideal crystal is

$$\beta F_0^{(R)} = \beta U_0(z) + 1 - 3/2 \ln(z) - A_1 z - A_2 z^2 - \tilde{w}. \quad (27)$$

Here we have $A_1 = a_1 \alpha^*/k$; $A_2 = a_2 (\alpha^*/k)^2 + A_1^2/2$; $\tilde{w} = \beta W$ is the dimensionless pair correlation contribution⁷. The quantity

$$\beta U_0 = \frac{3\pi S_n}{n(n-1)S_{n-2}z} \quad (28)$$

is the repulsive contribution to the energy of the static lattice, and $\alpha^*(\rho) = \alpha(\rho) a^2$ is the reduced elastic constant:

$$\alpha^*(\rho) = A_n \frac{n(n-1)}{6a^{n+2}} S_{n+2} = C_n \rho^{\frac{n}{3}} \quad (29)$$

where $S_n = \sum_{j>1} (\frac{a}{R_{1j}})^n$ are lattice sums [17].

Due to strong Coulomb attraction, neighbour ions are so close to one another that their electron shells significantly overlap. The Coulomb contribution $\Delta F_0^{(C)}$ corresponding to the zero-order approximation, i.e. to an ideal perfect crystal, is adequately represented by the Glauber–Yuchnovsky potential [18]:

$$\Delta F_0^{(C)} = -M \frac{e^2 Z^{(4+)} Z^{(2-)}}{4\pi \epsilon_0 a} (1 - e^{-bV^{1/3}}). \quad (30)$$

Here M is the Madelung constant, a is the lattice parameter and b is a screening constant treated below as an adjustable parameter.

6. Coulomb interaction of defects

Coulomb interaction of defects is complicated and its formulation is still a not well understood problem. On the one hand, defects belong to the lattice structure and should therefore be treated with conventional methods of solid-state physics. On the other hand, defects are relatively free to move and should be regarded, in a certain sense, as an ionic fluid component. The primary idea of the approximate method we used in this work is as follows: all charged species in the non-stoichiometric imperfect ionic solid are initially regarded as they would be in the fluid state. Thus, the Coulomb free energy of a ionic fluid mixture can be written in the form (see [10, 11] for details and references therein)

$$\beta \Delta F_C = \frac{\phi(\Gamma)}{72\eta}; \quad \Gamma \equiv \frac{\langle d \rangle}{r_D}; \quad r_D^{-2} = \frac{e^2}{\epsilon_0 V k T} \sum_{\alpha=1}^6 N_\alpha Z_\alpha^2. \quad (31)$$

In equation (31) and hereafter r_D is the Debye radius, Γ the Coulomb parameter, $\phi(\Gamma)$ a single-parameter (but quite general) Coulomb interaction function, $\eta = \pi n \langle d \rangle^3 / 6$ the packing

⁷ Note that in the quasi-harmonic approximation \tilde{w} does not depend on temperature and, therefore, is treated here as a constant.

fraction, σ_i the effective diameters of the charged particles (ion or vacancy) and $\langle d \rangle$ the mean size of the particle, defined by

$$\langle d \rangle^3 = \frac{\sum_i N_i \sigma_i^3}{\sum_i N_i}. \quad (32)$$

The value of the Coulomb parameter Γ in the condensed ionic phase is very high ($\Gamma \approx 40$ in liquid UO_2 near the melting point at $T_m = 3120$ K [11]).

The Debye–Hückel limiting law (DHLL): $\beta \Delta F_{\text{DHLL}}^{(C)} = -\Gamma^3$ appears to be very far from reality at such high densities. Much more accurate results of the integral equation theory [15] at $\Gamma \gg 1$ can be approximated by using the simple power form:

$$72\eta\beta\Delta F^{(C)} \approx -1.27\Gamma^{2.12}. \quad (33)$$

Since the concentration of defects is much lower than the concentration of lattice anions and cations, we can define a dimensionless parameter δ from $\Gamma^2 = \Gamma^2(x = \varphi = \varepsilon = 0)(1 + \delta)$ or

$$\delta = \sum_{i=0,1,3,5} N_i Z_i^2 \left(\sum_{i=2,4,6} N_i Z_i^2 \right)^{-1}$$

which is smaller than unity. Indices 0, 1, 3 and 5 correspond to all charged quasi-particles considered as defects (see table 1). Expanding the free energy equations (31) and (33) in powers of this parameter we get:

$$\Delta F^{(C)} = \Delta F_0^{(C)} (1 + \delta)^{1.06} \approx \Delta F_0^{(C)} + 1.06\Delta F_0^{(C)}\delta + \dots \quad (34)$$

We assume $\Delta F_0^{(C)}$ to be a sum of interactions of type equation (30) for all ionic pairs considered in the regular lattice sites. At the same time, we retain the ‘fluid-like’ form of the second term in equation (34).

Note that the term in equation (34) linear in δ is proportional to $-V^{-0.06}T^{-1.06}$. This volume dependence of $\Delta F_0^{(C)}$ is small but not negligible. The weak decrease of this term with increasing volume corresponds to the slight increase of the (negative) energy of Coulomb interaction between defects with increasing density. This explains the observed increase in density of the solid with the U/O ratio⁸.

According to equation (34), the Coulomb contribution to the Helmholtz free energy formally depends on the effective charges of all species (e.g., for UO_{2+x} it includes seven values of effective charge, $Z_0 \dots Z_6$). However, not all of them can be regarded as independent parameters.

Applying the electro-neutrality condition together with the requirement of invariability of the effective charges Z_i , we obtain four additional constraints and, hence, only three effective charges (e.g., for UO_{2+x} , Z_2 , Z_3 and Z_4 may be used as EOS parameters). The final equation for the Coulomb contribution to the interaction of defects has the following form:

$$\Delta F_{x,\varphi,\varepsilon}^{(C)} = \Delta F_0^{(C)} (V_0) \left(\frac{Z_4}{4} \right)^2 \left(\frac{V_0}{V} \right)^{0.06} (C_x x + C_\varepsilon \varepsilon + C_\varphi \varphi), \quad (35)$$

⁸ See the kink of the non-stoichiometric solid density as a function of temperature in figure 1.

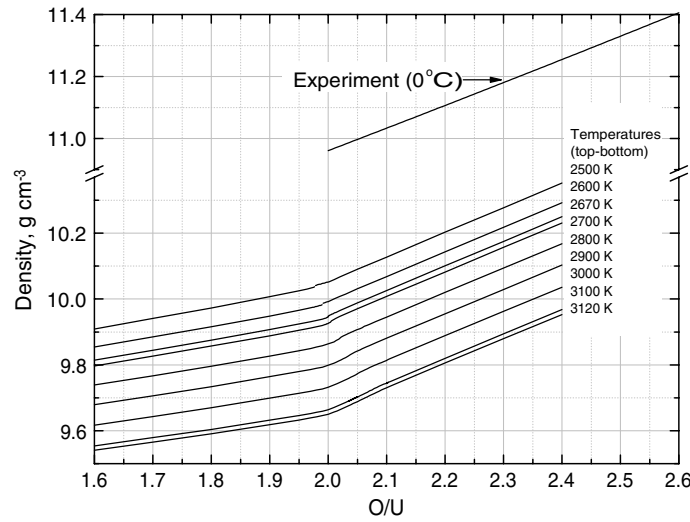


Figure 1. Density of non-stoichiometric UO_2 solid. The kink of the $\rho(T)$ dependence is associated with the Coulomb interaction of defects.

where V_0 is an arbitrary reference value of volume. For UO_{2+x} , three coefficients C_x , C_ε , and C_φ , are determined by three effective charges Z_2 , Z_3 and Z_4 :

$$\begin{aligned} C_\varepsilon &= \frac{(Z_4 - Z_3)^2}{2Z_2Z_4 + Z_4^2 + 3Z_2^2}; \\ C_\varphi &= \frac{2(Z_4 - Z_3)(3Z_2 - 2Z_3 + 3Z_4)}{2Z_2Z_4 + Z_4^2 + 3Z_2^2}; \\ C_x &= \frac{2(Z_4 - Z_3)(2Z_5 - Z_3 - Z_4)}{2Z_2Z_4 + Z_4^2 + 3Z_2^2}. \end{aligned} \quad (36)$$

7. Anharmonic effects in imperfect crystal

Formation of Frenkel defects is related to effective displacements of ions comparable, in the order of magnitude, with the lattice parameter a . The variation of the potential energy in such displacements cannot be described within the model of quasi-harmonic forces. Furthermore, vacancy formation affects the crystal force field in such a way that the usual anharmonicity phenomena considerably change.

Short-range repulsion forces in an ideal lattice determine the anharmonicity of the crystal force field. Usually, this contribution is negative and inversely proportional to the elastic constant, leading to a small negative effect on the heat capacity [15]:

$$\begin{aligned} \beta \Delta F_{\text{anh}}^{(R)} &= -A_1 z \sim -T/\alpha(\rho); \\ A_1 > 0 \quad \Delta C_{V \text{ anh}} &< 0. \end{aligned} \quad (37)$$

Apart from displacements of adjacent ions from the equilibrium positions, the anharmonic contribution to the force field is changed by formation of vacancies. The potential becomes 'flatter', and the sign of the anharmonic contribution changes. We adopt here the following

simplified form for additional anharmonic contribution, proportional to the concentration of vacancies:

$$\begin{aligned}\beta \Delta F_{\text{anh}}^{(R)} &= -(A_1 + \alpha_1 \varphi) z; \\ A_1 &> 0; \quad \alpha_1 < 0.\end{aligned}\tag{38}$$

Here α_1 is treated as an empirical constant to be fitted from existing experimental data.

8. Short-range interaction of defects

Coulomb interaction of defects is the principal, but not sole, contribution to the defect interaction. Another important kind of interaction is due to the short-range component of the inter-ionic forces. We consider a vacancy as a quasi-particle having short-range attractive interaction with neighbouring ions, and an interstitial as an additional centre of short-range repulsion placed in a non-occupied interstitial site.

Short-range interaction of two Frenkel defects is very much like the interaction of two electric dipoles. Two interstitials, as well as two vacancies, repel whilst vacancies and interstitials attract each other. Contrary to point charge interaction, electric dipole interaction decreases very fast with increasing distance. For an inverse-power site–site interaction, the ‘dipole–dipole’ pair potential⁹ has the form

$$\Phi(r, \theta_1, \theta_2, \phi) = \frac{n(n+1)A_n}{r^{n+2}} (2 \cos \theta_1 \cos \theta_2 - \sin \theta_1 \sin \theta_2 \cos \phi). \tag{39}$$

Here θ_1 , θ_2 , and ϕ are the polar and azimuthal angles between the axes of two quasi-dipoles.

This short-range interaction is actually important only for nearest interstitial ions and vacancies. Long-ranged Coulomb interaction is responsible for the energy of the defect formation, but their mutual orientation is sensitive to the short-range interaction. Two quasi-dipoles tend to orient themselves, whenever it is possible, as electrical dipoles do: ‘head to tail’. Yet, the constraints imposed by the lattice do not allow them exactly this orientation since there are only a few possible directions for the axis of quasi-dipoles, e.g. along the spatial crystalline directions of the cubic structure. For an isolated defect four possible orientations are equally probable. Formation of a vacancy promotes the displacement of neighbouring ions, and the probability of formation of a second defect in the vicinity of the existing one increases.

The contribution of the interaction of two neighbouring defects to the free energy of the imperfect crystal is negative. At the same time, the higher the concentration of defects, the larger is the positive contribution to the interaction of quasi-dipoles in their non-favourable orientations. The accurate theoretical description of the defect formation and interaction in non-stoichiometric solids is a problem still to be solved. In the next section we describe a new model for description of interaction between defects, which was previously proposed by the authors [19].

9. Defect interaction and order–disorder transition

Experimental evidence on the nature of the oxygen defect interaction in UO_2 is firstly provided by their pronounced tendency to form complexes [7, 20]. In the hyperstoichiometric dioxide solid solution up to moderately high temperatures, these interactions cause formation

⁹ It should be noted that the distance between vacancy and interstitial forming a Frenkel defect is always comparable with the distance between centres of interacting defects. Therefore, the scheme of point dipoles can be applied only for qualitative estimations.

of phases characterized by ordering of the extra oxygen atoms in anion superstructures with cell sizes as large as four times that of the fcc cation lattice.

Furthermore, in the stoichiometric dioxide the enthalpy versus temperature curve at high temperatures indicates an excess contribution that was initially attributed to oxygen defects created by a single-energy thermally activated process [21]. The effective role of oxygen defects was confirmed by neutron diffraction studies showing an upswing in the oxygen Frenkel pair concentration at temperatures between 2000 and 2700 K [22]. It was, however, Bredig [23] who, after examining the local trend of $H = H(T)$ in the range 2600–2700 K suggested the presence of a lambda transition at 2670 K. Since the defect concentration increase across this transition was as high as 20–30% of the oxygen sub-lattice sites, he considered this effect as a pre-melting transition produced by co-operative interactions of oxygen Frenkel pairs. This transition separates a high-temperature crystal state characterized by a large disorder in the anion sublattice from the ‘ordered’ low-temperature state, where the concentration of defects obeys the ‘regular’ thermodynamic equilibrium.

In fact, these phenomena are not rare in ionic crystalline solids (especially in those crystallizing in a fluorite or anti-fluorite lattice) and are mostly experimentally observed in the form of superionic conduction transitions.

The analysis of these effects presents some difficulties, as the classical Debye–Hückel shielding theory is unable to correctly reproduce the experiment. Thus more complex formulations of defect interactions have been proposed. It was, however, realized that in all cell models the distance of closest approach together with the Debye length represent the crucial quantities [24]. A copious literature has been published on this subject. Available microscopic models were therefore tested and applied to describe the pre-melting transition in UO_2 . These models are essentially based on semi-empirical expressions of the defect free energy of formation, containing a negative interaction term varying with the defect concentration [25–27] or with the hydrostatic strain produced by the defects [28].

More comprehensive evidence on the pre-melting transition in UO_2 was later provided by the work of Hiernaut *et al* [8] and Ronchi [29], where the behaviour of C_p across the transition was detected by a thermal arrest method in samples of different stoichiometry. These experiments showed that in the stoichiometric dioxide a sharp transition occurs at 2670 K, whilst no heat capacity singularity is observed in the hyperstoichiometric oxide. On the other hand, for hypostoichiometric compositions a sharp transition was detected at higher temperatures (up to 2950 K).

These authors explained the behaviour of the pre-melting transition in UO_{2+x} adopting a mean-field model where the defect interaction was expressed as a quadratic term in their concentration, and the coupling coefficient was fitted to produce a second-order transition at 2670 K in the stoichiometric oxide. Application of the model to non-stoichiometric compositions leads for $x > 0$ to the disappearance of the transition with a broadening of the heat capacity peak. For increasing x this peak continuously evolves from the C_p singularity occurring at $x = 0$ (we call this process ‘diffusive transition’ since its behaviour is analogous to that of a system whose partition function for internal energy is defined by two states separated by an energy gap of the order of magnitude of kT). On the other hand, for $x < 0$ a discontinuity of the defect concentration across a distinct temperature is predicted, indicating the occurrence of a first-order transition.

Though apparently successful in describing the features of the Bredig transition in the non-stoichiometric oxide, the formulation of this model presents the evident shortcoming that the assumed defect contribution to internal energy is supposed to describe defect long-term interactions without any explicit account of short-range interactions. Consequently, in its basic formulation the model predicts defect concentrations well above the experimental

values. In response to this, the aforementioned authors included in the configurational entropy a phenomenological ‘site-blocking’ parameter [30] simulating the effect of repulsive short-range interaction.

A more straightforward approach is assumed here, based on the considerations of the preceding section, where it is shown that the short-range interactions can be described with a tractable formalism deduced from simple physical hypotheses. To reproduce the physical picture described in terms of quasi-dipole interactions, one should take into account, at least, pair and triple interactions of defects, i.e., represent the contribution of the short-range interaction of defects in stoichiometric solid as

$$\beta \Delta F_{\text{int}}^{(R)} = -A_2 \varphi^2 + A_3 \varphi^3. \quad (40)$$

The pair interaction is proportional to φ^2 , and corresponds to the attraction of quasi dipoles, while the triple one is proportional to φ^3 and describes the repulsion effect (we suppose that both coefficients A_2 and A_3 are positive). As the concentration of vacancies increases, the (negative) value of $\beta \Delta F_{\text{int}}^{(R)}$ decreases, its magnitude reaches a minimum at some concentration φ_{max} and at a concentration φ_0 turns again to zero. At this concentration the short-range attraction between quasi-dipoles in favourable orientations is counterbalanced by the repulsion of quasi-dipoles in non-favourable orientations. At higher concentrations, the total short-range defect interaction become positive, i.e., repulsion dominates.

We use the simplest analytical form for A_2 and A_3 compatible with general properties of the inter-defect interaction described above, namely

$$A_2 = A_{20} + A_{21}/kT, \quad (41)$$

$$A_3/A_2 = B \simeq \text{constant}, \quad (42)$$

where constants A_{20} , A_{21} and B must be deduced from existing experimental data¹⁰.

We applied here an additional simplification by setting $A_3/A_2 = 2 - x$. This choice corresponds to the minimum of $\beta F_{\text{int}}^{(R)}$ at $\varphi_{\text{max}} = 1/3$ for stoichiometric solid, and gives the following expression for the equilibrium constant of vacancy formation:

$$K_{\varphi}^{(2)} = K_{\varphi}^{(1)}(T, V) \exp \left\{ 2A_2(T) (\varphi - 3\varphi^2) \right\},$$

where

$$K_{\varphi}^{(1)}(T, V) = \exp \left\{ S^{(1)} - C_{\varphi} \frac{\Delta F_0^{(C)}(V_0)}{kT} \times \left(\frac{Z_4}{4} \right)^2 \left(\frac{V_0}{V} \right)^{0.06} - \alpha_1 z \right\} \quad (43)$$

is the equilibrium constant equation (9) calculated without the contribution of short-range inter-defect interaction. It plays the role of the ideal-gas equilibrium constant, while function $K_{\varphi}^{(2)}(T, V, \varphi)$ is the real equilibrium constant in the model (with interaction of defects). $S^{(1)}$ is the entropy of defect formation:

$$S_{\varphi}^{(1)} = \left(\frac{\partial \alpha(\rho, \varphi)}{\partial \varphi} \right)_{\varphi=0} + \left(\frac{\partial \tilde{w}}{\partial \varphi} \right)_{\varphi=0}, \quad (44)$$

$\Delta F_0^{(C)}(T, V_0)$ is the Coulomb contribution equation (30) to the energy of the ideal crystal (per uranium ion) at the reference volume V_0 , C_{φ} is defined by equation (36), α_1 is the vacancy contribution to the anharmonic correction, $z = \{\beta \alpha^*(\rho)\}^{-1}$ and $\alpha(\rho)$ is the elastic constant equation (29).

The parameters α_1 and C_{φ} , even if fitted, are not independent empirical constants (as in conventional quasi-chemical models [12]) but must be seen as free energy parameters,

¹⁰ Within this model, we neglect the density dependence of constants A_{20} and A_{21} and set the value $B = 2$ (for stoichiometric UO_2).

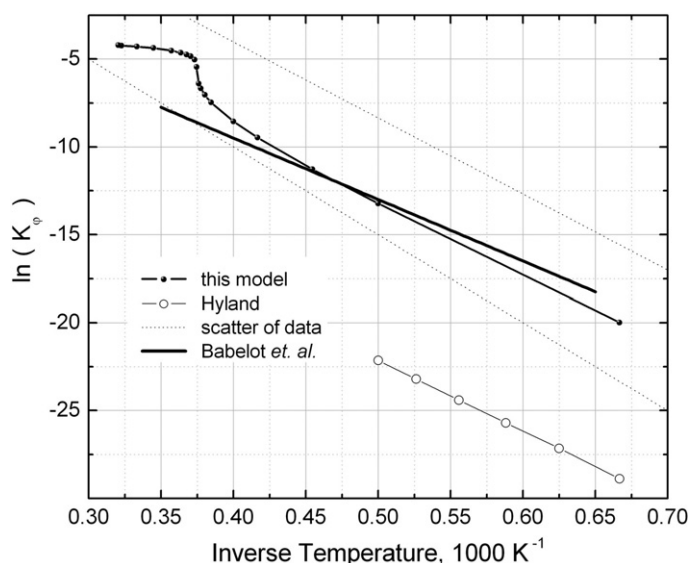


Figure 2. Equilibrium constants of defect formation in non-stoichiometric solid.

whereby their values obviously also affect other solid properties. For example, the entropy of the stoichiometric solid depends on the value of α_1 and the heat capacity is strongly affected by the value of C_φ . This gives us an additional mean to check the self-consistency of the model.

It is possible to fit the parameters in equation (43) to reproduce empirical values of equilibrium constants K_ε and K_φ known from literature [7, 12, 31] and then use them to predict other properties of the solid. Thus the model self-consistency was checked after choosing different sets of parameters to describe the temperature dependence of the equilibrium constants.

Two sets of parameters are compared in figure 2 respectively proposed by Hyland [12] and by Babelot *et al* [31]. The disagreement between the two estimates is remarkable. Though starting from almost the same values of the reaction heat, they differ by four orders of magnitude in the equilibrium constant. At low temperatures, far from the λ -transition, Hyland's version of the model gives much less satisfactory predictions of entropy and heat capacity than the model calibrated according to the recommendations of Babelot *et al* [31]. At the same time, the low-temperature data on oxygen potential as a function of O/U at small stoichiometry deviations are in better agreement with the recommendations of Hyland [12]. Keeping in mind the priority requirement of self-consistency of the model applied, we do not include below the recommendations of [12] as an essential constraint.

Using the equation of mass action law, equation (7), we can solve it with respect to x :

$$x = 1 - \varphi - \frac{\varphi}{\varphi + (2 - \varphi) K_\varphi^{(1)} \exp \{2A_2 (\varphi - 3\varphi^2)\}}.$$

The $x(\varphi)$ function behaves like the well known van der Waals isotherm $P(V)$. At low temperatures (or at large values of $K_\varphi^{(1)}$) the $x(\varphi)$ -relationship becomes non-monotonic: it decreases abruptly for small values of φ , then reaches a minimum, it increases again until it reaches a maximum, and finally decreases to the asymptote $x = -\varphi$ at larger values of φ . Thus, at some intermediate temperature (or at some intermediate value of $K_\varphi^{(1)}$) the $x(\varphi)$

function behaves like the critical van der Waals isotherm. Two ‘critical conditions’ are held for a certain value $x = x_C$:

$$\left(\frac{\partial x(\varphi)}{\partial \varphi} \right)_{\varphi=\varphi_C} = 0; \quad (45)$$

$$\left(\frac{\partial^2 x(\varphi)}{\partial \varphi^2} \right)_{\varphi=\varphi_C} = 0. \quad (46)$$

This ‘critical point’ is a location of a second-order phase transition akin to the λ -transition in fluorite structures. Since, according to the experimental observation, this transition takes place in stoichiometric UO_2 , we can add the third ‘critical condition’:

$$x_C = 0 \quad \text{and} \quad T_C = 2670 \text{ K}. \quad (47)$$

The equations for the three critical conditions equations (45)–(47) were solved to determine three unknown parameters of the model, $K_\varphi^{(1)}$, A_2 and φ_C :

$$\left(K_\varphi^{(1)} \right)_{\varphi=\varphi_C} = \frac{\varphi_C^2}{(1 - \varphi_C)(2 - \varphi_C)}; \quad (48)$$

$$A_2 = \frac{4 - 3\varphi_C}{2\varphi_C(2 - 15\varphi_C + 19\varphi_C^2 - 6\varphi_C^3)}. \quad (49)$$

We obtain the value of φ_C as the solution of the algebraic equation:

$$54\varphi_C^4 - 210\varphi_C^3 + 273\varphi_C^2 - 120\varphi_C + 8 = 0.$$

Substituting the result into equations (48) and (49), we get finally

$$A_2 = 25.5834;$$

$$\left(K_\varphi^{(1)} \right)_{\varphi=\varphi_C} = 1.61446 \times 10^{-4},$$

$$\varphi_C = 0.0805228;$$

This value of the ‘critical concentration’ of Frenkel defects φ_C is in good agreement with the neutron diffraction data [22].

10. Frenkel disorder: phase transition and phase equilibrium

The second order transition in stoichiometric uranium dioxide is an assumption inferred from experimental observations. Furthermore, if the model is applied to non-stoichiometric oxides, the predictions are qualitatively in agreement with the results of Hiernaut [8]. However, the question of whether or not the phase transitions predicted by the model coincide with the observed transitions in UO_{2+x} is not a simple one. Stability or instability of the oxygen sublattice in given experimental situations depends not only on the behaviour of its free energy, but also on the interrelation of characteristic times of measurement and diffusion related phenomena. If the time of experiment τ_M is essentially shorter than the characteristic diffusion time τ_D , phase transitions in solid occur like polymorph transitions in one-component crystals related to loss of stability of existing crystalline structure, i.e., almost instantly, without separation into two phases of different elemental composition¹¹.

¹¹ In this context it is worthwhile noting that in the laser-pulse experiments carried out to investigate the Bredig transition [8] this was always produced in UO_2 samples sintered at low densities, whilst in high-density samples the transition appeared only after several repeated shots. This observation was made by the authors of the above mentioned article with the remark that high porosity favours homogeneous sample vaporization, and hence minimizes possible composition gradients. Yet, in the light of the present analysis, the suppression effect can be more realistically attributed to the difficulty of producing a sufficiently rapid bulk expansion in dense samples, compared to the case where large sintered porosity makes it much easier.

This regime of ‘frozen diffusion’ is like the ‘forced congruent mode’ in solid–liquid or liquid–vapour transitions (see [11]). To avoid confusion about this kind of transitions, we shall refer below to this regime for Bredig-like transitions as the ‘fast transition mode’ (FTM).

The opposite limiting case corresponds to long time of measurement and/or to very fast diffusion processes. We shall refer to this regime, where $\tau_M \gg \tau_D$, as the ‘phase equilibrium mode’ (PEM). In the case of PEM, only the behaviour of the free energy of the solid determines the kind of phase transition, and its minimum with respect to the concentration of possible phases is the prevailing criterion. The characteristic diffusion time $\tau_D = L^2/D$ depends on a size L depending on the macroscopic structure of the sample and on the diffusion coefficient D . In measurements based on quenching or laser impulses, experimental conditions are probably closer to the FTM than to the PEM regime. In this regard, some predictions made for the FTM regime are discussed here below. This means that we are looking for (partial) equilibrium corresponding to a minimum of free energy with respect to internal variables (φ, ε) at given P, T and U/O ratio.

For non-stoichiometric solid the above scheme should be extended to account for additional dependence on stoichiometry. The final equation adopted for the short-range contribution $\Delta F_{x,\varphi,\varepsilon}^{(R)}$ is as follows:

$$\Delta F_{x,\varphi,\varepsilon}^{(R)} = \Delta F_{\text{anh}}^{(R)} + \Delta F_{\text{int}}^{(R)} + C_{xx}x^2, \quad (50)$$

where $\Delta F_{\text{int}}^{(R)}$ is the defect interaction contribution equation (40), $\Delta F_{\text{anh}}^{(R)}$ is the anharmonic correction equation (38), and the value of the empirical constant C_{xx} is to be established from experimental data.

11. Calibration procedure

The problem of calibration of a many-parameter non-linear EOS is considerably complex. Usually, the results of calibration depend on the form of functional involved in the minimization procedure (e.g., least squares estimators) as well as on the set of experimental data chosen. Normally, it is impossible to prove the uniqueness and global property of the found functional minimum. Therefore, additional criteria such as the correspondence to the limiting case of the ideal solid and the reasonable values of the parameters found may become important. A two-step calibration procedure was adopted. In the first step the parameters for the stoichiometric compounds were determined, and, subsequently, the parameters related to non-stoichiometric states were fixed. The sensitivity study performed has shown that the results are almost insensitive to values of some parameters. For example, any value of parameter n in equation (26) in the range from 5 to 12 leads to almost the same predicting quality. This is apparently related to the narrow range of inter-ionic distances corresponding to the experimental range of densities considered. The value of this parameter was eventually fixed at $n = 9$. The second anharmonic parameter A_2 appears to be insignificant and was set to zero.

Five parameters were fitted in the first calibration step (imperfect stoichiometric crystal): C_n , equation (29); B , equation (30); A_1 and W , equation (27); α_1 , equation (38). The following known properties of solid UO_2 (at zero pressure) were used:

- density as a function of temperature ($1500 \text{ K} < T < 3120 \text{ K}$);
- Gibbs potential at the melting temperature;
- entropy at the melting temperature and at $T = 2500 \text{ K}$.

In the second step, the remaining parameters (effective charges Z_2, Z_3, Z_4 and C_{xx}) have been determined by using

Table 2. Parameters of EOS within model of imperfect and non-stoichiometric solid.

Parameter	Value	Source
C_n/k	1.24×10^7 K	Density, Gibbs potential
B	$0.41 \text{ (cm}^3/\text{mol)}^{1/3}$	and entropy of
W	-0.23	stoichiometric solid
A_1	7.9	
α_1	92.0	
Z_2	-2.24	Oxygen pressure,
Z_3	2.52	concentration of vacancies
Z_4	3.85	and pressure of uranium
C_{xx}/k	2×10^4 K	vapour at triple point

Table 3. Adopted parameters of the λ -transition and defect interaction.

Parameter	Description	Value
T_C	Temperature of transition in stoichiometric solid	2670 K
H_f	Enthalpy of vacancy formation	3.67 eV
S_f/R	Entropy of vacancy formation	7.22
A_{20}	Defect interaction (equation (41))	-37.8
A_{21}	Defect interaction (equation (41))	15 eV
B	Defect interaction (equation (42))	$2 + x$

- the estimated value of the oxygen pressure at $T_m(6 \times 10^{-5} \text{ bar})$,
- the concentration of vacancies at $T = 2700 \text{ K}$ [34] and
- the pressure of uranium vapour at the triple point $T = 2700 \text{ K}$ [32].

The results are presented in table 2.

The adopted model parameters, including the phase transition, are listed in table 3. We assumed the measured temperature of the pre-melting transition in stoichiometric solid UO_2 equal to $T_C = 2670 \text{ K}$, and the enthalpy of defect formation at this temperature $H_f = 3.67 \text{ eV}$. The corresponding entropy and equilibrium constant for formation have been determined from the critical conditions equations (45)–(47). These data were used to fit the values of the effective charges of ions and vacancies. These values also determine the equilibrium constant for the disproportionation reaction equation (10). No additional parameters to describe the uranium disproportionation reaction were needed.

12. Comparison with experimental data and discussion

A comparison of the predictions of the present EOS with existing data for stoichiometric UO_2 solid is presented in table 4 and in figures 3 and 4.

The density of the stoichiometric solid in the temperature range 1500 K–3120 K is in good agreement with recommended data [32]. All examined model versions represent very well the temperature dependence of density for $x = 0$.

Predictions of the Gibbs potential are also in good agreement with the reference IVTAN database [32] over the temperature range 1500–3120 K (note that only one value (at T_m) was used for calibration).

Two values of entropy (at $T = 2500 \text{ K}$ and T_m) have been used for calibration. Good agreement of the data related to the defect interaction model and the IVTAN database is found except in the region close to the λ -transition temperature, since this transition was

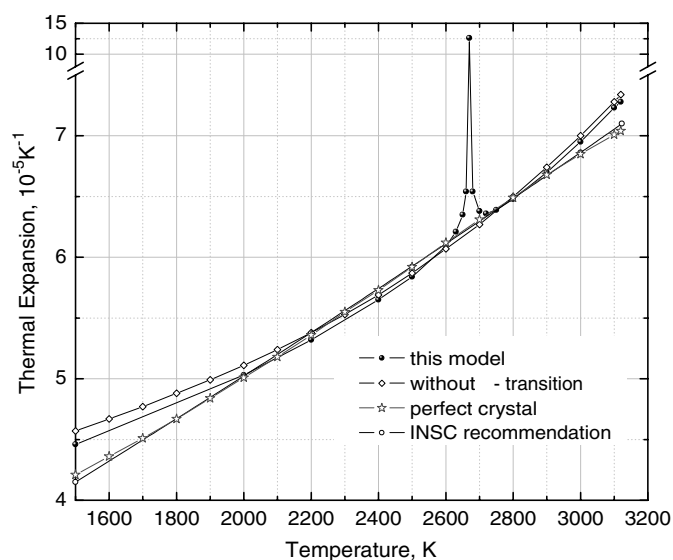


Figure 3. Expansivity of stoichiometric UO_2 solid. The sharp blip of the $\alpha_T(T)$ dependence is associated with the λ -transition.

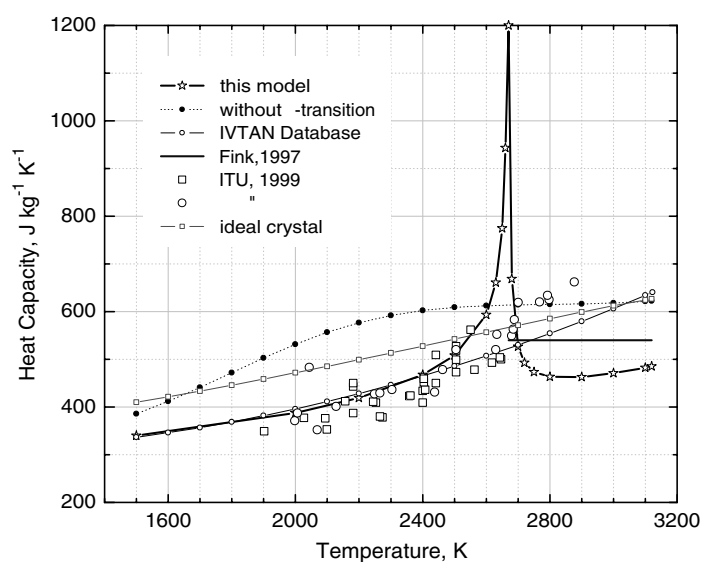


Figure 4. Heat capacity of stoichiometric solid.

not considered in the database. Consequently, the temperature dependence of the enthalpy exhibits similar deviations. In this view, the comparison of predicted and measured values of C_p presented in figure 4 is explanatory. We did not use C_p for calibration, leaving it for a check of the overall prediction quality.

The results are in good agreement with the experiments of Ronchi *et al* [8] at $T < 2670$ K, though lower values of C_p are predicted at higher temperatures.

Table 4. Thermodynamic properties of stoichiometric uranium dioxide at zero pressure as calculated from the imperfect-solid model. The potentials are referred to the pure ideal-gas ionic state of U and O. The data used for calibration are printed in bold characters.

T (K)	Density (g cm ⁻³)	δ (%)	α_T (10 ⁻⁵ K ⁻¹)	β_T (10 ⁻¹² Pa ⁻¹)	C_P (J kg ⁻¹ K ⁻¹)	G (kJ kg ⁻¹)	H (kJ kg ⁻¹)	S (kJ kg ⁻¹ K ⁻¹)
1500	10.573	-0.07	4.46	7.49	340.1	-8 528.6	-7385	0.7622
2000	10.326	0.00	5.03	8.30	387.6	-8 936.3	-7205	0.8658
2200	10.220	0.00	5.32	8.69	419.2	-9 113.3	-7124	0.9042
2400	10.108	-0.02	5.65	9.14	467.7	-9 298.0	-7036	0.9425
2500	10.050	-0.03	5.84	9.38	507.9	-9 393.2	-6987	0.9624
2600	9.991	-0.03	6.09	9.65	593.2	-9 490.5	-6933	0.9837
2630	9.972	-0.03	6.21	9.73	661.0	-9 520.1	-6914	0.9908
2650	9.960	-0.03	6.35	9.79	775.0	-9 540.0	-6900	0.9962
2660	9.953	-0.03	6.54	9.82	943.5	-9 550.0	-6892	0.9994
2670	9.946	-0.01	—	9.86	—	-9560.0	-6 872	1.0068
2680	9.939	0.00	6.54	9.89	668.6	-9 570.1	-6861	1.0108
2700	9.926	0.00	6.38	9.95	526.5	-9 590.3	-6850	1.0151
2720	9.913	0.00	6.36	10.01	492.7	-9 610.7	-6839	1.0188
2750	9.894	0.00	6.39	10.10	473.3	-9 641.3	-6825	1.0241
2800	9.863	0.00	6.48	10.26	463.1	-9 692.7	-6802	1.0325
2900	9.798	0.00	6.70	10.59	462.8	-9 796.8	-6755	1.0487
3000	9.731	0.01	6.95	10.96	471.0	-9 902.5	-6709	1.0646
3100	9.663	0.02	7.23	11.35	482.5	-10 009.7	-6661	1.0802
3120	9.649	0.03	7.28	11.44	485.3	-10 031.3	-6651	1.0833

The correct approximation of the crystal density guarantees the overall good reproduction of the thermal expansion coefficient as a function of temperature. At the same time, the model predicts a narrow and high peak in the vicinity of the λ -transition (see figure 3). Unfortunately, sufficiently accurate values of the crystal compressibility are not available for comparison. Nevertheless the agreement with best estimates [33] is satisfactory.

Predictions of the present EOS for non-stoichiometric UO_{2+x} are presented in figures 1 and 5. Only a few data are available for comparison. In figure 1 the density of the non-stoichiometric solid is plotted against the O/U ratio. The solid black line in the hyperstoichiometric region represents Perio's empirical equation [35]

$$a(\text{\AA}) = 5.4690 - 0.12x, \quad (51)$$

deduced from experimental data at $T = 273$ K. The predicted behaviour of the solid density is very similar to that observed at low temperatures.

There are no discontinuities in the Gibbs potential dependence except for small kinks at concentrations corresponding to the λ -transition. The behaviour of the oxygen potential for non-stoichiometric solid UO_{2+x} is presented in figure 6. The curves are plotted over an O/U range where existence of a solid solution is experimentally proved. A few comments are here in order concerning the predicted behaviour of the oxygen equilibrium pressure at lower temperatures. Some curves exhibit a negative slope in a distinct O/U interval ending with a minimum. This interval corresponds to metastable states. Only at higher O/U does the oxygen pressure become monotonically increasing. In this interval of instability two phases may be formed separated by a first-order transition.

The concentration of vacancies φ in the FTM regime exhibits remarkable discontinuities in the transition point ($\varphi = 0.108$ in the 'disordered phase' and $\varphi = 0.0593$ in the 'ordered phase', i.e., is about 50% less). The density as a function of composition presents

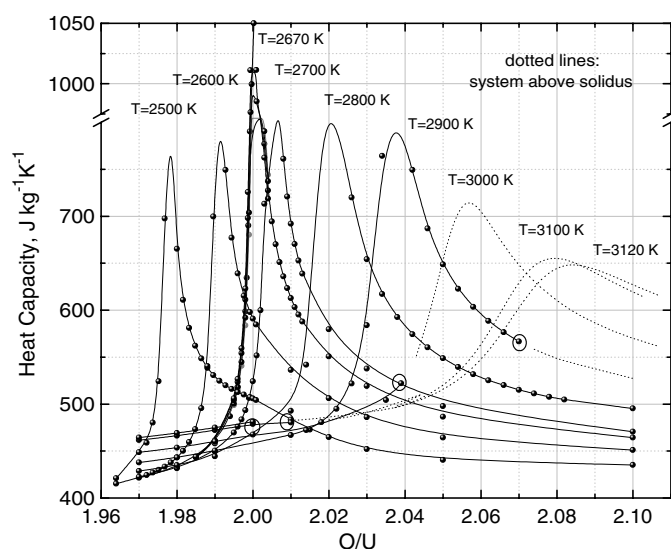


Figure 5. Heat capacity of non-stoichiometric solid. The locus of the C_p maxima is referenced here as a line of diffuse transition.

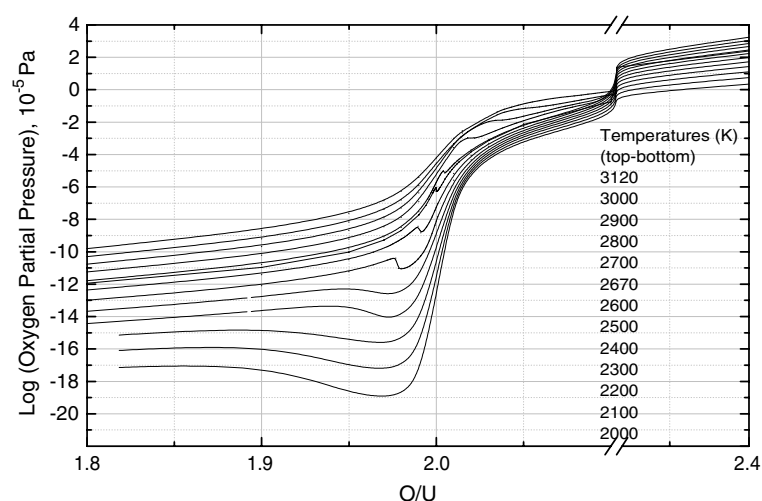


Figure 6. Oxygen potential of non-stoichiometric UO_2 solid.

discontinuities as well, but they are relatively small ($\rho = 9983 \text{ kg m}^{-3}$ in the ‘ordered phase’ and $\rho = 9987 \text{ kg m}^{-3}$ in the ‘disordered phase’, i.e., 0.04%).

For hyperstoichiometric compositions the model predicts no λ -transition but a ‘diffuse transition’, in accordance with the experimental observation. The points of maximal heat capacities on the isotherms are shown in figure 5. The lines of the λ - and diffuse transitions are plotted in figure 7. The solid line corresponds to the λ -transition in the FTM regime, the dashed one to the location of the diffuse transition. The vertical bars represent the concentration of the coexisting phases in the PEM regime. The cross ($T = 2904 \text{ K}$, $\text{O/U} = 2.0366$) indicates the predicted hypothetical PEM critical point.

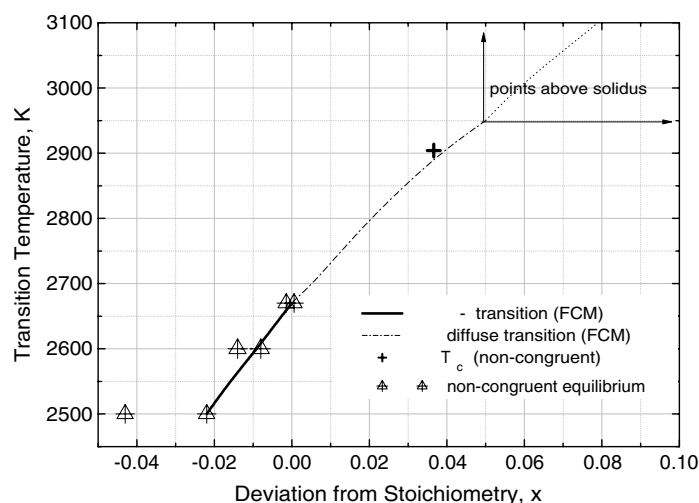


Figure 7. λ - and diffuse transitions in non-stoichiometric solid.

13. Conclusions

A general model for the Helmholtz free energy of non-stoichiometric imperfect solids was developed, applied and tested on UO_{2+x} . The adopted variational approach enables the thermal, caloric and oxidation properties of non-stoichiometric solids to be described with a single EOS model. This also makes it possible to express the equilibrium constants both of defect formation and of disproportionation reactions in an explicit form, by using analytical expressions for the free energy.

A general equation for the 'oxygen potential' was derived, and the behaviour of the oxygen pressure in both hypo- and hyperstoichiometric regions of UO_{2+x} can be predicted.

The approximate method to account for Coulomb interaction of defects provides explicit expressions for its contribution to the free energy of imperfect and non-stoichiometric solid, depending on the effective charges of ions and vacancies.

The model was extended to include short-range interactions between defects in imperfect solid UO_{2+x} . Frenkel defects were treated as quasi-dipoles with short-range attractive interactions between vacancies and interstitial ions and short-range repulsion between two vacancies and two interstitials. This approach, adopted to analyse the concentration dependence of short-range inter-defect forces, represents a basic underlying feature of the defect interaction model. The model describes this physical configuration in terms of quasi-dipoles taking into account pair and triple short-range interactions. Under some conditions, it predicts a 'critical point' which can be regarded as a second-order phase transition akin to the λ -transition observed in fluorite structures. These conditions were analysed and parameters of the model and phase transition have been determined.

A two-stage calibration procedure was developed for the non-stoichiometric solid model, and the EOS parameters have been determined by fitting existing experimental and reference data, so that the EOS correctly predicts the behaviour of the thermodynamic functions in non-stoichiometric and imperfect ionic solid, including the pre-melting λ -transition.

In particular, the density, Gibbs energy, entropy, thermal expansion and oxygen potential of non-stoichiometric UO_{2+x} have been compared with experimental data. Heat capacity and compressibility have been used for testing the overall quality of the model predictions.

A few words are finally in order concerning the adopted formulation of the defect interactions.

The approximate equation (40) is actually valid only in the stoichiometric case; it was, however, slightly modified by introducing a stoichiometry dependence of parameter B (table 3). The value of the constant A_2 in equation (40) was deduced from experimental data of the stoichiometric dioxide, but the parameters A_{20} and A_{21} defining its temperature dependence, equation (41), are still unknown. This point is important since different choices of A_{21} lead to different functional dependences of $T_C(x)$ in the non-stoichiometric solid. Unfortunately, we still do not have sufficient experimental data on this dependence [8]. Therefore, the crucial empirical aspects of the model are mainly associated with the values of A_{20} and A_{21} listed in table 3. Though we believe that the proposed equations (39)–(41) are physically sound, the values of these parameters might need a revision if some new data on the $T_C(x)$ dependence are available in the future. As for the present state of experience and comprehension, the current calibration seems to be more appropriate for hyperstoichiometric than for hypostoichiometric uranium dioxide.

Acknowledgment

This collaboration work was made possible by the European Commission Programme on Research and Training on Nuclear Energy.

References

- [1] Manara D, Ronchi C and Sheindlin M 2002 *Int. J. Thermophys.* **23** 1171
- [2] Manara D, Ronchi C and Sheindlin M 2003/2004 *High Temp.–High Pressures* **35/36** 25
- [3] Latta R E and Fryxell R E 1970 *J. Nucl. Mater.* **35** 195
- [4] Chevalier P-Y, Fischer E and Cheynet B 2002 *J. Nucl. Mater.* **303** 1
- [5] Guéneau C, Baichi M, Labroche D, Chatillon C and Sundman B 2002 *J. Nucl. Mater.* **304** 161
- [6] McQueen R G 1991 *High-pressure Equation of State: Theory and Applications* ed S Eliezer and R A Ricci (Amsterdam: Elsevier) pp 101–216
- [7] Sørensen O T 1981 *Non-Stoichiometric Compounds* (New York: Academic) pp 1–59
- [8] Hiernaut J P, Hyland G and Ronchi C 1993 *Int. J. Thermophys.* **14** 259
- [9] Matveev L V and Veshchunov M S 1997 *Sov. Phys.—JETP* **111** 585
- [10] Ronchi C, Iosilevski I and Yakub E 1999 *INTAS Report Project 93-66* INTAS Brussels
- [11] Ronchi C, Iosilevsky I and Yakub E 2004 *Equation of State of Uranium Dioxide* (Berlin: Springer)
- [12] Hyland G J 1984 *Report EUR 9410* EN European Commission Karlsruhe, Germany
- [13] Shekatolina S A and Yakub L N 1976 *Fiz. Tverd. Tela* **18** 3137 (in Russian)
Shekatolina S A and Yakub L N 1976 *Ukr. Phys. J.* **21** 535 (Engl. Transl.)
- [14] Gryaznov V 1998 *Strongly Coupled Coulomb Systems* ed G Kalman and K Blagoev (New York: Plenum) p 147
- [15] Gryaznov V, Iosilevski I, Yakub E and Ronchi C 2000 *J. Physique IV* **10** 5 363
- [16] Girifalco L A 2000 *Statistical Mechanics of Solids* (Oxford: Oxford University Press)
- [17] Barker J A 1963 *Lattice Theories of the Liquid State* (Oxford: Pergamon)
- [18] Glauber A E and Yukhnovskii I R 1953 *Dokl. Akad. Nauk SSSR* **93** 999
- [19] Yakub E, Ronchi C and Iosilevski I 2003 *11th Int. Workshop on the Physics of Non-Ideal Plasmas* (Valencia, Spain, March 2003)
- [20] Willis B T M and Hazell R G 1980 *Acta Crystallogr. A* **36** 582
- [21] Szwarc R 1969 *J. Phys. Chem. Solids* **30** 705
- [22] Hutchings M T 1987 *J. Chem. Soc. Faraday Trans. II* **83** 1083
- [23] Dworkin A S and Bredig M A 1968 *J. Chem. Phys.* **72** 1277
- [24] March N H and Tosi M P 1981 *J. Phys. Chem. Solids* **42** 809
- [25] Hubermann B A 1974 *Phys. Rev. Lett.* **32** 1000
- [26] Welch D G and Dienes G J 1977 *J. Phys. Chem. Solids* **38** 311
- [27] Oberschmidt J 1981 *Phys. Rev. B* **23** 5038

- [28] Rice M J, Stressler S and Toombs G A 1974 *Phys. Rev. Lett.* **32** 596
- [29] Ronchi C and Hyland G J 1994 *J. Alloys Compounds* **213/214** 159
- [30] Speiser R and Spretnak J W 1955 *Trans. AIME* **47** 493
- [31] Babelot J-F, Ohse R W and Hoch M 1986 *J. Nucl. Mater.* **137** 144
- [32] Gurvich L V, Veyts I V and Medvedev V A 1996 *Thermodynamic Properties of Individual Substances* vol IV (Moscow: Nauka) (in Russian)
- [33] INSC ANL Material Properties Database <http://www.insc.anl.gov/matprop> Argonne National Laboratory, Illinois, USA
- [34] Iosilevski I, Hyland G J, Ronchi C and Yakub E 2001 *Int. J. Thermophys.* **22** 1253
- [35] Perio P 1955 Contribution to the crystallography of the uranium–oxygen system *Doctoral Dissertation* University of Paris CEA-363